Dyes and Pigments 191 (2021) 109366

Contents lists available at ScienceDirect

Dyes and Pigments

journal homepage: http://www.elsevier.com/locate/dyepig

Real-time tracking of lipid droplets interactions with other organelles by a high signal/noise probe

Wei Ren [a,1], Dong Wang [a,1], Wei Huang [a,1], Jiajia Li [a], Xiaohe Tian [a], Zhengjie Liu [a], Guangmei Han [a], Bianhua Liu [c], Ming-Yong Han [c], Zhongping Zhang [a,b], Ruilong Zhang [a,b,*]

[a] School of Chemistry and Chemical Engineering, And Institute of Physical Science and Information Technology, Anhui University, Hefei, 230601, China
[b] Key Laboratory of Structure and Functional Regulation of Hybrid Materials (Anhui University), Ministry of Education, Hefei, Anhui, 230601, China
[c] Key Lab of Photovoltaic and Energy Conservation Materials, Institute of Solid State Physics, HFIPS, Chinese Academy of Sciences, Hefei, 230031, China

ARTICLE INFO

Keywords:
Hydrophobic probe
High signal/noise
Lipid droplets
Organelles interaction

ABSTRACT

Investigating the interactions between lipid droplets (LDs) and other organelles are greatly significant to the in-depth understand the physiology and pathology of LDs. Despite of commercial LDs probes available, the ER and other membrane structures are also stained due to their amphiphilicity, which limits their further applications. To address this issue, we herein report a highly hydrophobic fluorescent probe to specifically label intracellular LDs with high signal/noise ratio, avoiding undesirable staining of ER and thus achieving to real-time monitor the interactions between LDs and other organelles. The probe showed strong emission in lipid environments but no fluorescence in water and liposomes, enabling the probe with high signal/noise ratio. Using this probe, it was found that the contacts of LDs with ER and mitochondria clearly increased under the condition of starvation.

1. Introduction

Lipid droplets (LDs) are key organelles in mammalian cells, which not only store most of lipids in living cells [1], but also exchange fat molecules to mitochondria [2,3], endoplasmic reticulum (ER) [4–8], and other membrane-structural organelles, especially under starvation or drug stimulation. In LDs, there is a hydrophobic phase of neutral lipids as the core covered by a monolayer membrane of phospholipids [9,10]. On the membrane of LDs, various lipoproteins are embedded to catalyze the lipolysis [11–13] and participate in the interactions between LDs and other organelles [5,14]. For instance, upon cell starvation, triacylglycerol (TG) in LDs is rapidly hydrolyzed to supply fatty acids to mitochondria where the energy is generated for the metabolisms of cells [15]. Under the nutrient-rich condition, TG accumulates in phospholipid layer of ER and forms a bent ER surface, and then is transported into LDs or forms a new LD [16]. In the case of ER stress, the LDs can also provide the raw materials to ER for phospholipid synthesis such as diacylglycerol (DG), to supply the consumption of the phospholipid in the process of ER autophagy [17]. Accordingly, the study of LD communication with other organelles is greatly significant to deeply understand the physiology and pathology of LDs [18].

The traditional method of observing LDs is transmission electron microscopy (TEM) [3,19,20], which has high resolution to show the ultrafine structure but incapable of distinguishing multiple lipid environments and tracking the dynamic of LDs in live cells. In this context, fluorescent imaging with high sensitivity and selectivity has become a powerful tool to real-time track LDs' behaviors [21,22]. To date, a large number of probes have been exploited and fabricated to label LDs [23–25], and parts of them have already been commercialized, e. g. BODPY 493/503 and Nile Red. However, most of the probes can also stain other hydrophobic environments such as phospholipid layer, making the investigation of the communication between LDs and other organelles difficult. Therefore, improving LDs-specific fluorescent probes with signal/noise ratio is critical to address this issue.

Herein, we report a highly hydrophobic probe which exhibits aggregation caused quenching (ACQ) to specifically label intracellular LDs (Scheme 1). The probe showed negligible fluorescence in water and liposomes, and thus avoided the staining of other membrane-structural organelles, realizing the real-time tracking of the interactions between LDs and other organelles. Further, we have demonstrated the contacts of

* Corresponding author. School of Chemistry and Chemical Engineering, and Institute of Physical Science and Information Technology, Anhui University, Hefei 230601, China.
E-mail address: zrl@ahu.edu.cn (R. Zhang).
[1] These authors contributed equally to this work.

https://doi.org/10.1016/j.dyepig.2021.109366
Received 23 February 2021; Received in revised form 30 March 2021; Accepted 1 April 2021
Available online 3 April 2021

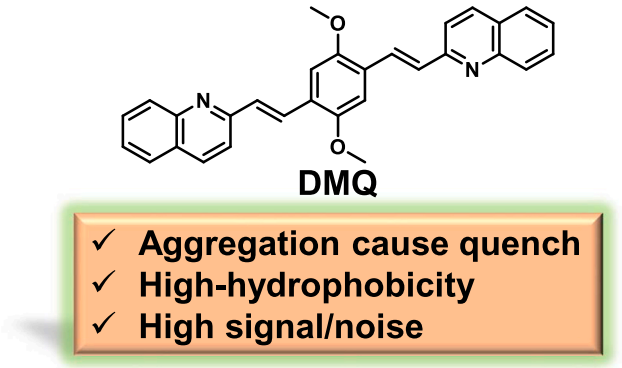

Scheme 1. The chemical structure of DMQ and its properties.

LDs with mitochondria and ER under the condition of starvation.

2. Experimental section

Regents and instruments. Glycerol trioleate (TG), glyceryl dioleate (DG), cholesterol (CE), cholesteryl ester (CH), oleic acid (OA), *p*-dianisole, *para*-formaldehyde, formaldehyde solution, triphenylphosphine and so on were purchased from Sigma. 3-(4,5-dimethythiazol-2-yl)-2,5-diphenyl tetrazolium bromide (MTT), BODIPY 493/503, ER-tracker Red and Mito-tracker DeepRed were purchased from Thermofisher. Other chemical reagents were obtained from Sinopharm Chemical Reagent Co., Ltd. Water was doubly distilled and purified via a Milli-Q water system (Millipore, USA). NMR spectra in solution were performed on Bruker 400 MHz Ultrashield Spectrometer. High-resolution mass spectra (HR-MS) were obtained by using an LTQ Orbitrap XL hybrid FTMS by Thermo Fisher Scientific. UV–visible absorption spectra were measured with a HITACHI UH5300 spectrometer. Fluorescent spectra were recorded on HITACHI F-7000 fluorescence spectrophotometer. Fluorescent images were acquired on laser confocal microscope (Leica TCS SP8X), and 50% of laser power was applied.

Synthesis of compound DMQ. The compound **a** and **b** were synthesized according to the reported method [26,27].

*Synthesis of compound **a**.* The *p*-dianisole (5.55 g, 40.2 mmol) and *para*-formaldehyde (1.52 g) were added into a 500 mL round bottom flask, followed by adding aqueous formaldehyde solution (30%, 12.5 mL), concentrated hydrochloric acid (140 mL) and 1,4-dioxane (32.0 mL). After refluxing for 6 h, the mixture was cooled and filtered to obtain the white precipitation as the crude product. The obtained powder was dissolved into CH_2Cl_2, and then MeOH (600 mL) was added, the white precipitation which was collected by filtration and air dried to afford compound **a** (7.18 g, yield 76%). ^{1}H NMR (400 MHz, $CDCl_3$) δ 6.93 (s, 2H), 4.64 (s, 4H), 3.86 (s, 6H). HR-MS (*m/z*, ESI) Calculated for $C_{10}H_{12}Cl_2O_2$ [M+H] *m/z* = 235.0287. Found *m/z* = 235.0276.

*Synthesis of compound **b**.* Compound **a** (2.6 g, 11.1 mmol), triphenylphosphine (8.8 g, 33.4 mmol) and methanol (70 mL) were added into a 250 mL round bottom flask, and then the mixture was refluxed for 8 h. After cooling down and removing the solvent in vacuum, a yellow oil was obtained. Toluene (200 mL) was added to the foregoing mixture and the generated white precipitation was filtered as the compound **b** (6.1 g, yield 72%). ^{1}H NMR (400 MHz, $CDCl_3$) δ 7.79–7.61 (m, 30H), 6.92 (s, 2H), 5.25 (d, *J* = 12.9 Hz, 4H), 2.96 (s, 6H). HR-MS (*m/z*, ESI) Calculated for $C_{46}H_{42}O_2P_2^{2+}$ [M] *m/z* = 344.1325. Found *m/z* = 344.1318.

*Synthesis of compound **DMQ**.* Firstly, Na (0.12 g, 5.22 mmol) was added to EtOH (14 mL) and stirred thoroughly until it was completely dissolved to obtain a solution of sodium ethoxide. Quinoline-2-formaldehyde (0.23 g, 1.46 mmol) and compound **b** (0.50 g, 0.66 mmol) were added into the above ethanolic solution of sodium ethoxide. After refluxed for 4 h, the solvent was removed by rotary distillation under vacuum. The solid was sequentially washed with *n*-hexane and water, and further purified by column chromatography eluent with CH_2Cl_2: MeOH (25:1, v/v). Finally, the orange solid was obtained as the final product, **DMQ** (0.19 g, yield 65%). ^{1}H NMR (400 MHz, $CDCl_3$) δ 8.11 (dd, *J* = 9.0, 14.1 Hz, 4H), 8.01 (d, *J* = 16.6 Hz, 2H), 7.80 (dd, *J* = 8.8, 15.7 Hz, 4H), 7.73–7.68 (m, 2H), 7.53–7.48 (m, 4H), 7.32 (s, 2H), 3.97 (s, 6H). ^{13}C NMR (101 MHz, $CDCl_3$) δ 156.61, 151.99, 148.18, 136.42, 129.88, 129.79, 129.10, 128.92, 127.61, 127.41, 126.79, 126.30, 118.81, 109.37, 77.42, 77.11, 76.79, 56.31. HR-MS (*m/z*, ESI) Calculated for $C_{30}H_{24}N_2O_2$ [M+H] *m/z* = 445.1911. Found *m/z* = 445.1902.

Quantum yield measure. The fluorescence quantum yields (Φ) of DMQ in different solvents were determined by using fluorescein (0.1 M NaOH, Φ = 0.95) as the standard reference, according to the literature method [28]. The quantum yields were corrected as follows:

$$\Phi_s = \Phi_r \frac{A_r D_s}{A_s D_r}$$

where the s and r indices refer to designate the sample and reference, respectively, A is the absorbance at λ_{ex}, and D is the integrated area under the spectrum.

Cell culture and MTT assay. All cells were cultured in culture flasks in DMEM (high glucose) supplemented with fetal bovine serum (10%), penicillin (100 U/mL) and streptomycin (50 U/mL) at 37 °C in a CO_2 incubator (95% relative humidity, 5% CO_2). Cells were seeded into 20 mm glass-bottomed dishes, and cultured for 24 h for fluorescent imaging.

The cytotoxicities of DMQ was studied by MTT assay. Hep G2 and HeLa cells (10^5 cell/mL, 10 mL) were dispersed with 96-well microtiter plates to a total volume of 100 μL/well. Plates were maintained at 37 °C in 5% CO_2/95% air incubator for 24 h. The cells were incubated for 18 h with different concentrations of DMQ (1, 2, 4, 6, 8 and 10 μM) in the medium at 37 °C. Then, 10 μL MTT (5 mg/mL) solution was added into each well and incubated for additional 4 h. After removal of supernatant and addition of 100 μL of DMSO into each well, the cells were shaken for 10 min, and the absorbance in each well was measured at 492 nm use of a microplate reader (Biotek, USA). The cell viability (%) was calculated according to the equation: cell viability % = A/B × 100%, where A represents the absorbance of each well treated with DMQ, and B represents that of the control wells.

3. Results and discussion

Firstly, we designed a highly hydrophobic probe, 2,2'-((1*E*,1'*E*)-(2,5-dimethoxy-1,4-phenylene)bis(ethene-2,1-diyl))diquinoline (DMQ). The synthetic route was shown in Scheme 2, and the structure of the target probe DMQ with a large π-conjugation was fully confirmed by HR-MS, ^{1}H and ^{13}C NMR (Fig. S1-S3). In the structure of DMQ, there was no strong hydrophilic moiety such as hydroxyl and amino groups (Scheme 1). We further measured the oil-water separation coefficient (log P) of DMQ as 3.034 (Fig. S4), suggesting our probe DMQ with high hydrophobicity. Then, the optical properties of DMQ in different solvents were tested (Fig. 1). In the absorption spectra, DMQ in PBS buffer (pH 7.2) showed a red-shifted peak and a broader band (Fig. 1a), likely because of the aggregation formation of DMQ in aqueous solution (Fig. S9). Meanwhile, DMQ had obvious fluorescence in different organic solvents but no emission in PBS buffer (Fig. 1b and Table 1), indicating that the aggregation of DMQ caused fluorescence quenching as a consequence of the formation of an exciplex (Fig. S9) [29,30]. Notably, DMQ had strong emission in TG, the major component of LDs core (Fig. 2a), which was the basis of label intracellular LDs. To ensure the low noise in the next imaging experiments, we further examined the DMQ fluorescent spectra in liposomes, similar to the membrane structures in live cells. The results indicated that no fluorescent signal was detected, which was like in PBS buffer. These results imply that our probe DMQ is a candidate for label LDs with high signal/noise ratio.

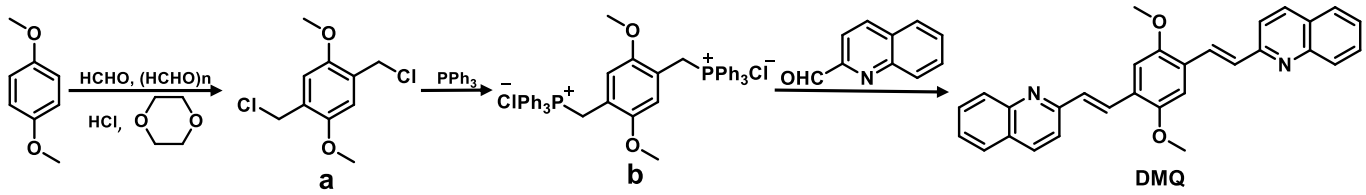

Scheme 2. The synthetic route of probe DMQ.

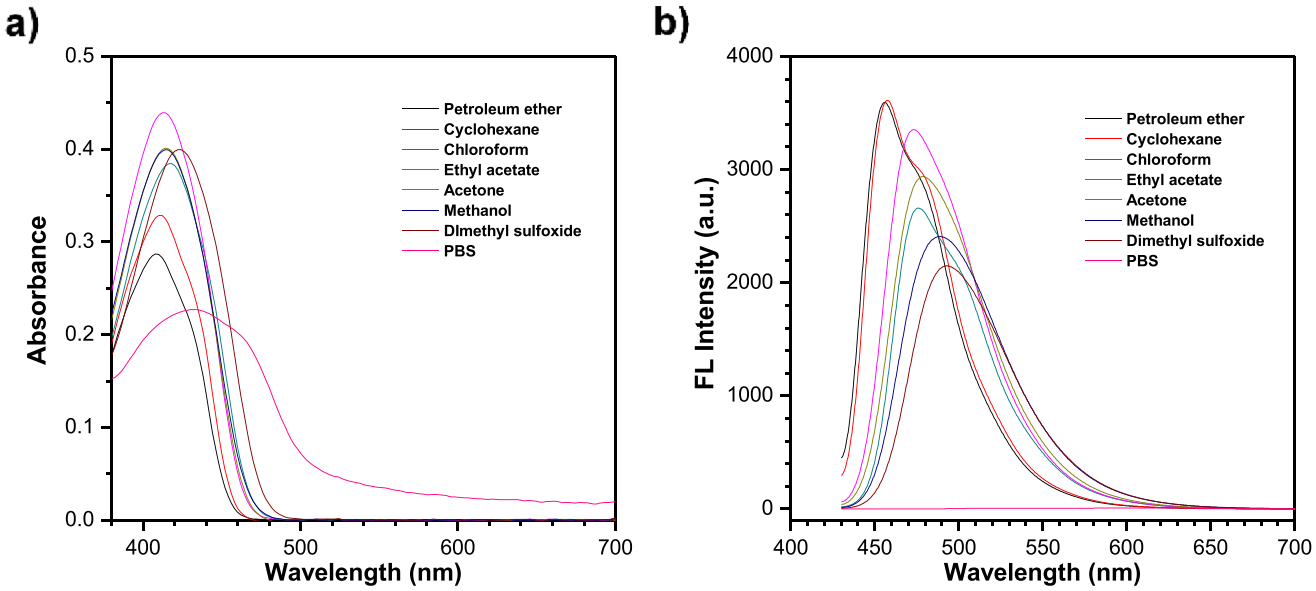

Fig. 1. (a) UV–vis spectra of DMQ in different solvents. (b) Fluorescent spectra of DMQ in different solvents.

Table 1
Summary of the absorbance maximum, emission peaks, Stokes' shift, the quantum yields of DMQ in different solvents.

Solvent	Absorbance (nm)	Emission (nm)	Stokes' shift (nm)	Φ
Petroleum ether	408.0	456.0	48.0	0.729
Cyclohexane	410.0	457.6	47.6	0.642
Chloroform	418.0	476.0	58.0	0.440
Ethyl acetate	414.0	473.0	59.0	0.494
Acetone	414.0	478.6	64.6	0.494
Methanol	414.0	488.6	74.6	0.440
Dimethyl sulfoxide	424.0	493.6	69.6	0.385
PBS	436.0	608.6	172.6	0.004

Next, we tested the fluorescence stability in the complicated bio-environments, because there are various reactive bio-species may interfere the fluorescence of DMQ. We added common biomolecules (including inorganic salts, amino acids, peptides, proteins, and nucleic acids) into DMQ aqueous solution, and found no obvious fluorescent change (Fig. S6). In parallel, we also investigated the fluorescence of DMQ in the presence of other components in LDs such as dioleate glyceryl (DG), oleic acid (OA), palmitic acid (PA), cholesterol (CE) and cholesterol ester (CH) (Fig. 2b), and the fluorescence of DMQ kept relatively steady. The above results showed that intracellular bio-molecules cannot interfere the DMQ emission, avoiding the generation of noise from biomolecules. Before moving to cellular imaging, the cytotoxicity of probe was measured by the classic MTT method (Fig. S7). The cell viability kept over 90% in the presence of 1–10 μM, indicating the almost non-cytotoxicity of probe.

For cell imaging, we set the imaging channel as excitation at 405 nm and emission collection in 450–550 nm. After the cells were incubated with 1 μM DMQ, the dot-like bright fluorescence was observed (Fig. 3a), and there was almost no noisy signal. To confirm that the fluorescent dots were LDs, the available commercial LD-tracker, BODIPY 493/503, was employed for the colocalization experiment (Fig. 3b and c). When the DMQ-loaded cells were further treated with 1 μM BODIPY 493/503, it was found that the fluorescent dots almost completely overlapped, suggesting the probe DMQ accumulated in intracellular LDs. The same results were obtained in other two cell lines (Fig. S8). It is worthy pointing out that the noise in Fig. 3b showed much stronger (Fig. 3d) but weaker LDs signal detected. The similar results were also observed by using Nile Red (Fig. 3e and j), suggesting that our probe DMQ had a higher signal/noise ratio due to the negligible fluorescence of probe in aggregation state and in liposomes. These results indicate the probe DMQ more suitable to investigate interactions between LDs and other organelles.

Next, we tried to use our probe to track LDs growth when the cells were treated with supplementary oleic acid (Fig. 4a). OA is an organic acid, and thus can be ionize partly in water and taken by cells. We have calculated the mean size of LDs, and the results were shown in Fig. 4b and c. It was found that the numbers and sizes of LDs exhibited the similar trend in the presence of oleic acid. In the initial stage, the LDs were relatively small with a mean area of 0.04 μm^2. In 0–2 h, the fluorescence intensity and size of LDs gradually increased under the treatment of oleic acid. Because DMQ with high hydrophobicity can easily accumulate into intracellular LDs, and the high concentration of DMQ in LDs may induces aggregation caused quenching (ACQ). With the uptake

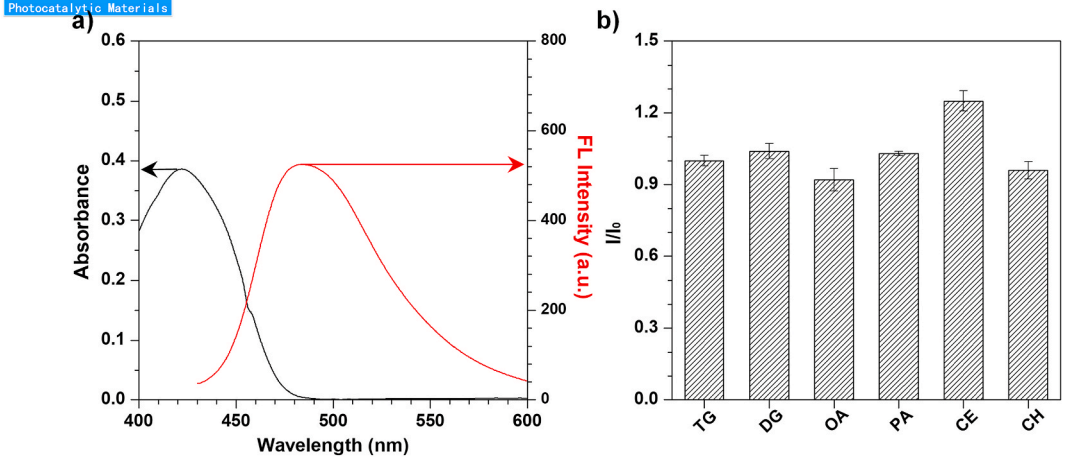

Fig. 2. (a) UV–Vis absorption and fluorescence spectra of DMQ (10 μM) in TG with the excitation of 405 nm, and collected in the range of 450–550 nm. (b) The fluorescence intensities at the emission peak (490 nm) of DMQ in different lipids environments. The different lipids environments contained 90% of TG and 10% other lipids, dioleate glyceryl (DG), oleic acid (OA), palmitic acid (PA), cholesterol (CE) and cholesterol ester (CH). The error bars represent mean errors from the results of three tests.

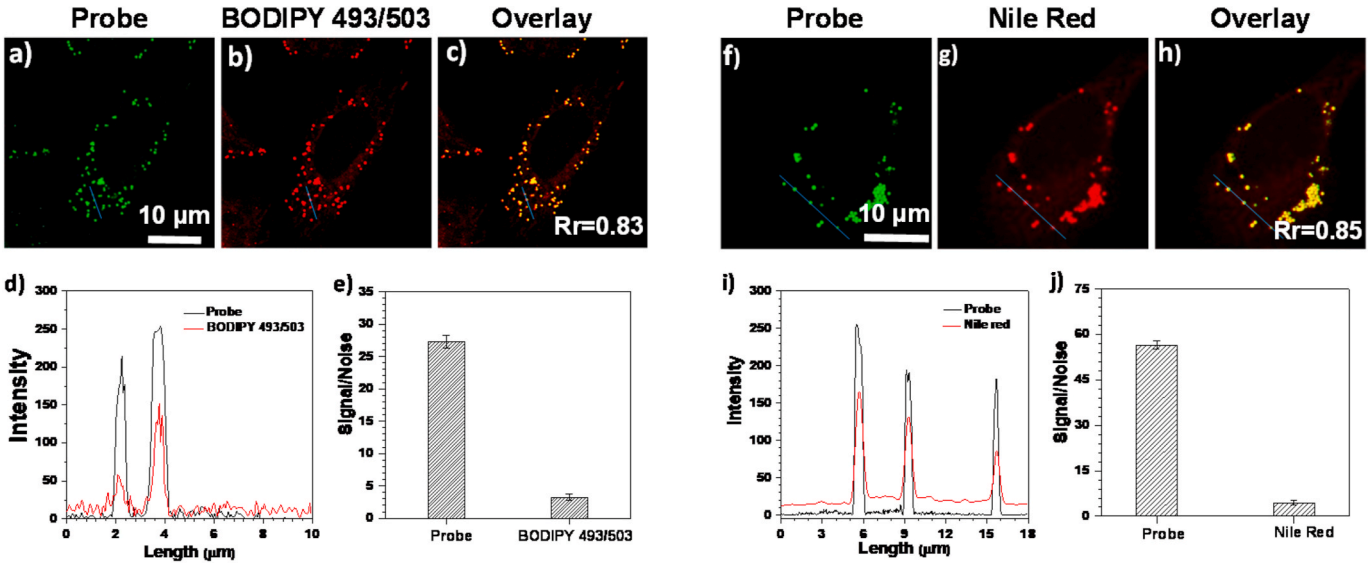

Fig. 3. Fluorescent images and profiles of Hep G2 cells stained with DMQ (1 μM) and BODIPY 493/503 or Nile Red (1 μM). The cells were incubated with DMQ for 20 min, and then treated with BODIPY 493/593 or Nile Red for another 20 min. (a) The image from DMQ channel. (b) The image from BODIPY 493/503 channel. (c) Overlay of (a) and (b). (d) Fluorescence intensity profile of region of interest (blue line in a and b). (e) Signal/noise ratios in (a) and (b). (f) The image from DMQ channel. (g) The image from Nile Red channel. (h) Overlay of (f) and (g). (i) Fluorescence intensity profile of region of interest (blue line in f and g). (j) Signal/noise ratios in (f) and (g). DMQ, BODIPY 493/503 and Nile Red were excited with 405, 493 and 550 nm, and collected in the range of 450–550, 500–550, and 600–650 nm, respectively. The error bars represent mean errors from the results of three tests.

of oleic acid, LDs' volume became bigger than before, resulting in the decrease of DMQ concentration and the increase of fluorescence intensity. In the period of 2–4 h, both the numbers and areas of LDs increased sharply, while the increase speed obviously decelerated after 4 h. The results showed that the sizes and numbers of LDs both increased upon the uptake of oleic acid (Fig. 4b and c), indicating that our probe DMQ was suitable to real-time monitor LD's growth in live cells. Interestingly, there was no detectable fluorescent signal in ER and other membrane-structural organelles, which further certifying that the probe DMQ can also be applied in the investigation of LDs contacting other organelles.

As well-documented, LDs as the source of intracellular lipids are often linked to other organelles, such as providing fatty acids to mitochondria and supplying lipid materials to ER in starvation condition [31]. To demonstrate these physiological behaviors, we employed the probe DMQ to study the interactions of LDs with mitochondria and ER. When we stained the cells with DMQ and Mito-tracker simultaneously, the LDs had no obvious communication with mitochondria, and their overlap coefficient as low as 0.03 (Fig. 5a). However, after the further incubation in nutrition-free media for 10 min, the overlap coefficient increased to 0.06, and rapidly enhanced 6-fold in another 1 h. In the control group of high glucose media, the overlap of LDs with mitochondria still kept in very low level (Fig. 5b and c). The results suggest that the more contacts occurred between LDs and mitochondria. In the case of DMQ and ER tracker, the similar results were also observed. Under the starvation condition, the overlap coefficient between LDs and ER also increased from 0.20 to 0.33, whereas the control group kept relative steady (Fig. 6). To confirm the results, we have using the

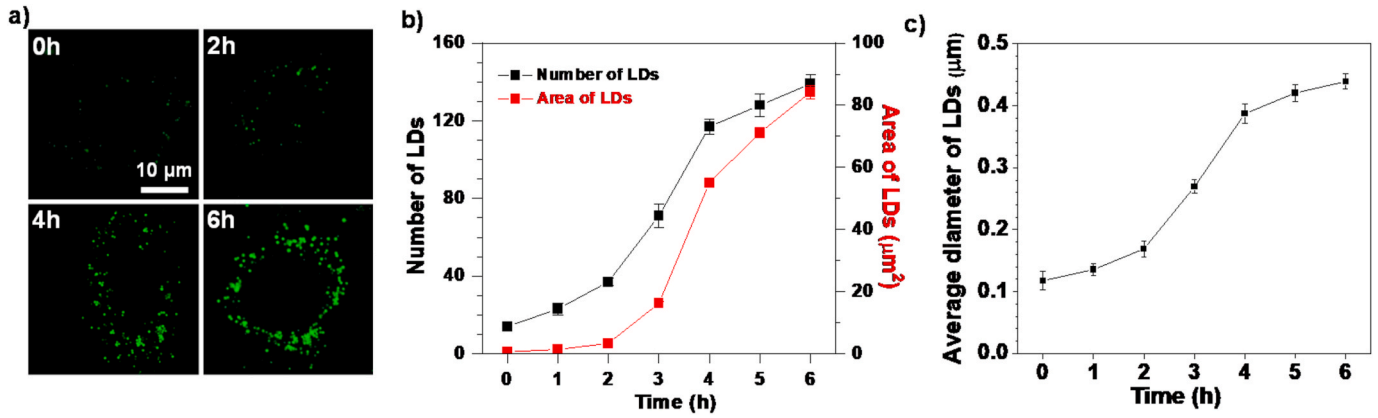

Fig. 4. (a) Fluorescence imaging of HeLa cells. The cells were first incubated with probe DMQ (1 μM), and then directly treated with 100 μM oleic acid (OA) for different times as indicated in the corresponding images. (b) Statics numbers and areas of LDs at different times. (c) Statics average diameter of LDs at different times. Here, DMQ were excited with 405 nm, and collected in the range of 450–550 nm. Error bars represent mean errors from the results of three tests.

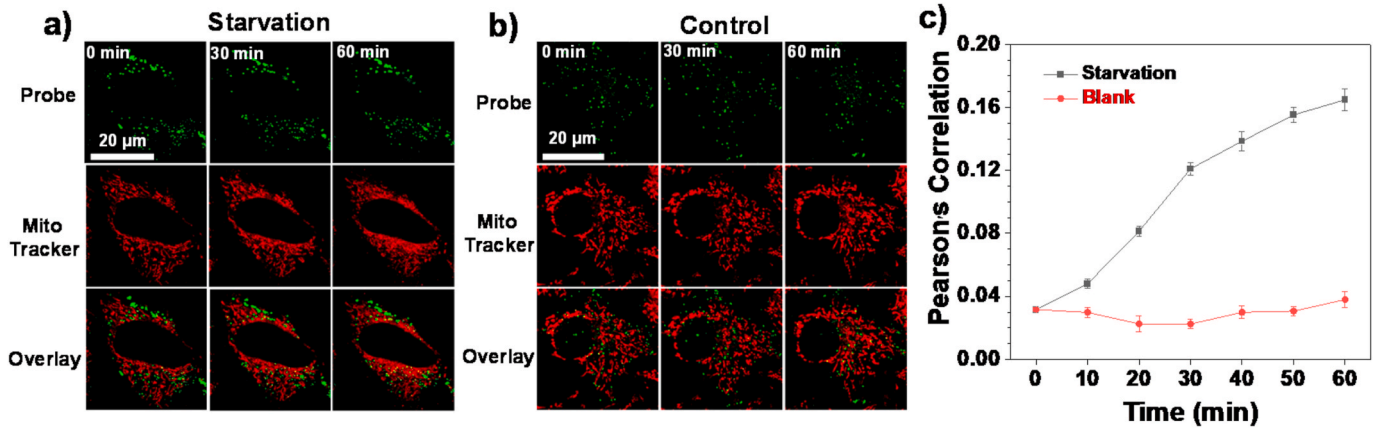

Fig. 5. Fluorescent imaging of the interactions between LDs and mitochondria. (a) Imaging of cells in starvation conditions. The cells were simultaneously incubated with DMQ (1 μM) and Mito-tracker Deep Red (1 μM) for 20 min, then cultured in 1.0 mL of serum-free Earle's balanced salt solution. (b) Imaging of control cells. The cells were simultaneously incubated with DMQ (1 μM) and Mito-tracker Deep Red (1 μM) for 20 min, then cultured in 1.0 mL of a nutrient-rich medium supplemented with 10% FBS. (c) The time-dependent Pearson's correlation of lipid droplets and mitochondria. Here, DMQ and Mito-tracker Deep Red were excited with 405 and 633 nm, and collected in the ranges of 450–550 and 645–665 nm, respectively. The error bars represent mean errors from the results of three tests.

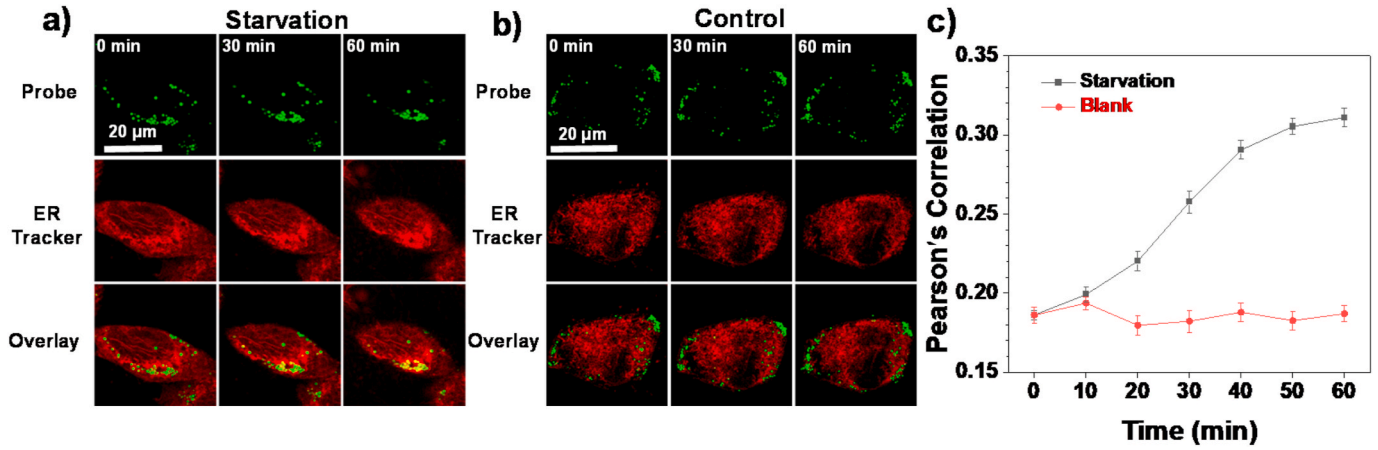

Fig. 6. Fluorescent imaging of the interactions between LDs and ER. (a) Imaging of cells in starvation conditions. The cells were simultaneously incubated with DMQ (1 μM) and ER-tracker Red (1 μM) for 20 min, then cultured in 1.0 mL of serum-free Earle's balanced salt solution. (b) Imaging of control cells. The cells were simultaneously incubated with DMQ (1 μM) and ER-tracker Red (1 μM) for 20 min, then cultured in 1.0 mL of a nutrient-rich medium supplemented with 10% FBS. (c) The time-dependent Pearson's correlation of lipid droplets and ER. Here, DMQ and ER-tracker Red were excited with 405 and 587 nm, and collected in the ranges of 450–550 and 600–650 nm, respectively. The error bars represent mean errors from the results of three tests.

commercial LDs dyes to carry out these experiments (Fig. S10 and S11), and the performance of commercial LDs dyes had the similar trends to that using our probe DMQ, but the overlaps of LDs and other organelles in the initial stage was higher, leading to the decrease of sensitivity. In particular, using BODIPY 493/503 (one of the commercial LDs dyes) had no enhancement in 0–20 min, which was contradictory to the fact. Together all, our probe with high signal/noise ratio was suitable to real-time monitor the interactions of LDs with other organelles in live cells.

4. Conclusions

In summary, we have developed a LDs-specific probe DMQ with high signal/noise ratio that can be used to real-time track the interplays of LDs with other organelles. The probe DMQ has no obvious fluorescence on aggregates and liposomes, so the signal of intracellular hydrophobic membrane structure can be ignored, thus avoiding the background fluorescence from membrane organelles such as ER. By the use of this probe, we have demonstrated that the contacts of LDs with mitochondria and ER increased under the starvation condition.

Author statement

Wei Ren: Methodology, Data curation; **Dong Wang:** Data curation; **Wei Huang:** Data curation; **Jiajia Li:** Data curation; **Xiaohe Tian:** Writing-Original draft; **Zhengjie Liu:** Cell culture; **Guangmei Han:** Imaging; **Ruilong Zhang:** Funding, Supervision, and Writing; **Bianhua Liu:** PI, Supervision, Funding, and Reviewing; **Ming-Yong Han**: PI, Supervision, Funding, and Reviewing; **Zhongping Zhang:** Funding, Reviewing and Editing.

Declaration of competing interest

The authors declare that they have no known competing financial interests or personal relationships that could have appeared to influence the work reported in this paper.

Acknowledgement

This work was supported by the National Natural Science Foundation of China (21775001, 21874137, 21974001, 21976183 and 22074001), Anhui Provincial Natural Science Foundation of China (1808085MB32).

Appendix A. Supplementary data

Supplementary data to this article can be found online at https://doi.org/10.1016/j.dyepig.2021.109366.

References

[1] Walther TC, Farese Jr RV. Lipid droplets and cellular lipid metabolism. Annu Rev Biochem 2012;81(1):687–714.
[2] Rambold Angelika S, Cohen S, Lippincott-Schwartz J. Fatty acid trafficking in starved cells: regulation by lipid droplet lipolysis, autophagy, and mitochondrial fusion dynamics. Dev Cell 2015;32(6):678–92.
[3] Cui L, Liu P. Two Types of Contact between lipid droplets and mitochondria. Front Cell Dev Biol 2020;8:618322–33.
[4] Markgraf DF, Klemm RW, Junker M, Hannibal-Bach HK, Ejsing CS, Rapoport TA. An ER protein functionally couples neutral lipid metabolism on lipid droplets to membrane lipid synthesis in the ER. Cell Rep 2014;6(1):44–55.
[5] Olzmann JA, Carvalho P. Dynamics and functions of lipid droplets. Nat Rev Mol Cell Biol 2019;20(3):137–55.
[6] Morris SNS, Olzmann JA. A tense situation: maintaining ER homeostasis during lipid droplet budding. Dev Cell 2019;50(1):1–2.
[7] Martin S, Driessen K, Nixon SJ, Zerial M, Parton RG. Regulated localization of Rab18 to lipid droplets: effects of lipolytic stimulation and inhibition of lipid droplet catabolism. J Biol Chem 2005;280(51):42325–35.
[8] Ozeki S, Cheng J, Tauchi-Sato K, Hatano N, Taniguchi H, Fujimoto T. Rab18 localizes to lipid droplets and induces their close apposition to the endoplasmic reticulum-derived membrane. J Cell Sci 2005;118(Pt 12):2601–11.
[9] Camus G, Schweiger M, Herker E, Harris C, Kondratowicz AS, Tsou CL, et al. The hepatitis C viruscore protein inhibits adipose triglyceride lipase (ATGL)-mediated lipid mobilization and enhances the ATGL iInteraction with comparative gene identification 58 (CGI-58) and lipid droplets. J Biol Chem 2014;289(52):35770–80.
[10] Londos C, Brasaemle DL, Schultz CJ, Segrest JP, Kimmel AR. Perilipins, ADRP, and other proteins that associate with intracellular neutral lipid droplets in animal cells. Semin Cell Dev Biol 1999;10(1):51–8.
[11] Sturley SL, Hussain MM. Lipid droplet formation on opposing sides of the endoplasmic reticulum. JLR (J Lipid Res) 2012;53(9):1800–10.
[12] Thiam AR, Farese JRV, Walther TC. The biophysics and cell biology of lipid droplets. Nat Rev Mol Cell Biol 2013;14(12):775–86.
[13] Chen D, Qin W, Fang H, Wang L, Peng B, Li L, et al. Recent progress in two-photon small molecule fluorescent probes for enzymes. Chin Chem Lett 2019;30(10):1738–44.
[14] Murphy S, Martin S, Parton RG. Lipid droplet-organelle interactions; sharing the fats. Biochim Biophys Acta Mol Cell Biol Lipids 2009;1791(6):441–7.
[15] Benador IY, Veliova M, Mahdaviani K, Petcherski A, Wikstrom JD, Assali EA, et al. Mitochondria bound to lipid droplets have unique bioenergetics, composition, and dynamics that support lipid droplet expansion. Cell Metabol 2018;27(4):869–85.e6.
[16] Datta S, Liu Y, Hariri H, Bowerman J, Henne WM. Cerebellar ataxia disease-associated Snx14 promotes lipid droplet growth at ER-droplet contacts. J Cell Biol 2019;218(4):1335–51.
[17] Li D, Yang S-G, He C-W, Zhang Z-T, Liang Y, Li H, et al. Excess diacylglycerol at the endoplasmic reticulum disrupts endomembrane homeostasis and autophagy. BMC Biol 2020;18(1):1–107.
[18] Fang Z, Su Z, Qin W, Li H, Fang B, Du W, et al. Two-photon dual-channel fluorogenic probe for in situ imaging the mitochondrial H2S/viscosity in the brain of drosophila Parkinson's disease model. Chin Chem Lett 2020;31(11):2903–8.
[19] Fujimoto T, Ohsaki Y, Suzuki M, Cheng J. Imaging lipid droplets by electron microscopy. Methods Cell Biol 2013;116:227.
[20] Sotiris J, Strong J, Sztalryd C, Hsia R-c. Studies of the interaction of cardiac lipid droplets with mitochondria using electron microscopy. Microsc Microanal 2014;20(S3):1376–7.
[21] He L, Cao J-J, Zhang D-Y, Hao L, Zhang M-F, Tan C-P, et al. Lipophilic phosphorescent iridium(III) complexes as one- and two-photon selective bioprobes for lipid droplets imaging in living cells. Sensor Actuator B Chem 2018;262:313–25.
[22] Li L, Xu Y, Chen Y, Zheng J, Zhang J, Li R, et al. A family of push-pull bio-probes for tracking lipid droplets in living cells with the detection of heterogeneity and polarity. Anal Chim Acta 2020;1096:166–73.
[23] Becerra-Ruiz M, Vargas V, Jara P, Tirapegui C, Carrasco C, Nuñez M, et al. Blue-fluorescent probes for lipid droplets based on dihydrochromeno-fused pyrazolo- and pyrrolopyridines. Eur J Org Chem 2018;2018(34):4795–801.
[24] Wang W, Han X-J, Liu J-T, Miao J-Y, Zhao B-X. A novel lipid droplets-targeted ratiometric fluorescence probe for HSO_3^-/SO_3^{2-} in living cells. Dyes Pigments 2020;173:107892.
[25] Cheng W, Xue X, Zhang F, Zhang B, Li T, Peng L, et al. A novel AIEgen-based probe for detecting cysteine in lipid droplets. Anal Chim Acta 2020;1127:20–8.
[26] Saikachi H, Muto H. Reaction of aromatic *p*-substituted bisphosphoranes with bisaldehydes. Chem Pharmaceut Bull 1971;19(5):959–69.
[27] Park YI, Kuo CY, Martinez JS, Park YS, Postupna O, Zhugayevych A, et al. Tailored electronic structure and optical properties of conjugated systems through aggregates and dipole-dipole interactions. ACS Appl Mater Interfaces 2013;5(11):4685–95.
[28] Mataga N, Kaifu Y, Koizumi M. Solvent effects upon fluorescence spectra and the dipolemoments of excited molecules. Bull Chem Soc Jpn 1956;29(4):465–70.
[29] Kuzmin MG. Exciplex mechanism of the fluorescence quenching in polar media. Pure Appl Chem 1993;65(8):1653–8.
[30] Epling GA, Lin Ki. Quenching of the fluorescence of quinoline derivatives by exciplex formation with heteroatom-containing compounds. J Heterocycl Chem 2010;21(4):1205–8.
[31] Pu J, Ha CW, Zhang S, Jung JP, Huh WK, Liu P. Interactomic study on interaction between lipid droplets and mitochondria. Protein Cell 2011;2(6):487–96.